Preparation of secondary gypsum binders from waste plaster molds of the ceramic industry and their properties

Abigail Parra Parra[1], Pedro Antonio Márquez Aguilar[1], Marina Vlasova[1*], Rosario Pochotitla Hernandez[1], Rene Guardián Tapia[1], Marcos Fuentes Perez[1]

[1]Center of Investigation in Engineering and Applied Sciences of the Autonomous University of the State of Morelos (CIICAp-UAEMor), Av. Universidad, 1001 Cuernavaca,México.

Abstract: *In the work, on the basis of results of XRD, IR spectroscopy, andSEM/EDS investigations, the process of phase transformations proceeding during temperature treatment of wastes of plaster molds from the ceramic industry has been considered. It has been established that the dehydration process of secondary $CaSO_4 \cdot 2H_2O$ occurs in the direction of the formation of secondary $CaSO_4 \cdot 0.5H_2O$ and $CaSO_4$ at a higher temperature than the dehydration of primary $CaSO_4 \cdot 2H_2O$.The shift of the dehydration temperature is ~100-150 °C. Treatment at 900–1000 °C is not accompanied by the formation of estrich gypsum and is characterized by defect formation in the lattice of $CaSO_4$. On the basis of secondary a soft-burned (200–300 °C) and a hard–burned (1000 °C) gypsum binders, and their mixtures, new gypsum materials possessing good strength properties are obtained without using primary gypsum binders.*

Key words:*gypsum waste, temperature treatment, binding properties, strength properties*

I. Introduction

Gypsum is finding extensive application in the building industry [1-6]. As a consequence, the production and use of gypsum products is accompanied by the accumulation of large volumes of wastes. One of the most important properties of gypsum waste is the relative simplicity of obtaining new binders, which are demanded in the building industry, from them. This is why, up to now, various flow diagrams for the manufacture of secondary gypsum binders depending on the properties of primary gypsum waste have been continuously developed [7-10].

In the manufacture of the most widespread commercial and construction gypsum binders, untreated calcium sulfate $CaSO_4 \cdot 2H_2O$, which is transformed into $CaSO_4 \cdot 0.5\ H_2O$ by heating in the temperature range 140–170 °C, is used (see **Fig 1**). Commercial calcium sulfate α-hemihydrate is widely used for the manufacture of molds for the pouring of clay slips in the production of sanitary, household, and art pottery of complex shape [11, 12]. At the same time, it should be kept in mind that, to dilute clays, solution of electrolytes (Na_2CO_3, Na_2SiO_3, and NaOH) with an initial concentration of 2% are used [13]. After multiple pouring processes of slips, such plaster molds gradually absorb water with electrolytes dissolved in it and transform into secondary $CaSO_4 \cdot 2H_2O$, lose their ability to absorb water, and become "wastes". In view of the large volume of such wastes, the necessity to develop a simple technology for their utilization arises.

The aim of the present work is to investigate phase transformations during temperature treatment of waste plaster molds of the ceramic industry and evaluate the binding properties of newly formed materials and the possibility of using them as new materials for the building industry.

II. Experimental

A processing scheme of waste plaster molds that includes milling of wastes, their temperature treatment, and preparation of dry mixtures and dough/pastes based on them is shown in **Fig. 2**.

Wastes of plaster molds were milled before and after temperature treatment in a Retsch Planetary Ball Mill PM 400/2 (Germany) in different regimes: v = 250–360 rpm and t = 3–10 min. Bottle cullet was milled at v= 360 rpm for10 min to obtain glass particles with of size $d \leq 70$ μm.

The milled plaster molds were subjected to temperature treatment in the range 100–1100 °C for 2 h at every temperature and then milled in the regime v = 300 rpm and t = 5 min. For subsequent investigations, powders with a particle size $d \leq 50$ μm were taken.

On the basis of gypsum powders subjected to low-temperature and high-temperature treatment and milled glass, dry mixtures were obtained. Water was added to the dry mixtures to prepare gypsum dough, from which bars with sizes 6 cm × 3 cm × 1.5 cm and 1 cm × 1 cm × 2 cm were made to perform compressive tests with the aim to determine compressive strength and fracture toughness. On the basis of the obtained results, mixtures that can have practical application in the building industry were chosen.

The particle-size distribution was assessed by screen analysis and with the help of a Laser Particle Sizer ANALYSETTE 22 COMPACT unit (Germany).

Physicochemical processes proceeding in the stage of temperature treatment of gypsum waste were analyzed on the basis of XRD, IR spectroscopy, and SEM/EDS data. XRD measurements were carried out on a Siemens D–500 X-ray diffractometer (Germany) in Cu Kα radiation. SEM/EDS data were obtained on a SEM/FIB NOVA 200 system (Bruker, Germany). Both local EDS analysis, and an investigation in the map mode over an area 9.556 × 9.556 μm^2 were performed. IR absorption spectra were recorded on a Specord M80 spectrometer (Germany). The compressive strength of specimens was determined according to ASTM[14], and the fracture toughness [15].

III. Results

3.1. Preliminary milling of wastes

Gypsum wastes broken into lumps were subjected to milling in different operational regimes of the ball mill. The most rational milling regime, which provided the mean particle size (d) of ~50 μm, was a rotational rate of 300 rpm and a milling time of 5 min (**Figs. 3 a, b**). With further increase in the milling time, an apparent increase of the particle size as a result of the aggregation of fine gypsum particles and their densification was noted. As a seen in **Figs. 3 c**, **c'**, in the milling regime with v = 300 rpm and t = 5 min, a polydisperse system containing both micro particles and coarser particles/aggregates forms. A substantial part of aggregates fractures easily during ultrasonic treatment (see **Figs. 3 c**, **c'**).

3.2. Temperature treatment of milled wastes

The temperature treatment of powdered wastes showed that with increase in T_{tr} up to 1100 °C, $(CaSO_4 \cdot 2H_2O)_{sec.}$ is gradually dehydrated and transforms into $CaSO_4$ via the stage of formation of $(CaSO_4 \cdot nH_2O)_{sec}$, where $n \leq 0.5$ (**Fig. 4**). The absence of peaks of CaO in the X-ray diffraction patters of hard-burned powders indicates that the content of calcium oxide (if it forms) is less than 5%. The difference of the phase transformations during temperature treatment of milled wastes from those for the primary calcium sulfate dehydrate[16, 17] is the shift to of the temperature of the complete transition of $(CaSO_4 \cdot 2H_2O)_{sec}$ into $(CaSO_4 \cdot 0.5H_2O)_{sec/}$ and $CaSO_4$ to the higher temperatures, the extension of the regions of coexistence of $(CaSO_4 \cdot 2H_2O)_{sec}$ + $(CaSO_4 \cdot nH_2O)_{sec}$ and $(CaSO_4 \cdot 0.5H_2O)_{sec}$ + $CaSO_4$, and the absence of CaOappearance, which correspond to the decomposition/dissociation of $CaSO_4$ in the temperature range 900–1100 °C (see **Fig. 5**).

In the IR absorption spectra, the dehydration process of $(CaSO_4 \cdot 2H_2O)_{sec}$, is observed in [18-21]. It characterized by a decrease in the intensity of O–H bonds in the ranges ν~ 3550–3390 cm^{-1} and ν~ 1680–1620 cm^{-1} (see **Fig. 5** and **Table 1**) at T_{tr}=100–500 °C. The absorption bands in the ranges ν~ 1150–500 cm^{-1} and ν~

674–590 cm^{-1} correspond to Ca–SO_4 bonds, i.e., to the formation of $CaSO_4$. The narrowing of the intense band at ν~1100 cm^{-1} indicates that, in the powders treated at 600–800 °C, the structure of the anhydrite $CaSO_4$becomes gradually more perfect. However, at T_{tr} > 800 °C, this band begins to broaden, which testifies to the process of defect formation in the crystal lattice of calcium sulfate, that precedes the decomposition/dissociation of $CaSO_4$ and subsequent formation of CaO with increase in T_{tr}[22].

Thus, according to the XRD and IR spectroscopy data, during temperature treatment of the investigated gypsum waste, the dehydration process of $(CaSO_4 \cdot 2H_2O)_{sec}$and its gradual transition into calcium sulfate hemihydrate (bassanite) and then into anhydrite occur at higher temperatures than those for primary gypsum (see **Fig. 6**).

The microphoto shows (**Fig. 7 a**) that the crushed powder $(CaSO_4 \bullet 2H_2O)_{seq}$ consists of particles of different sizes and shapes, which is consistent with the data presented in **Fig. 3 c**.With increase in the treatment temperature of the gypsum waste powder, further refinement of the polydisperse system is observed up to T_{tr}~ 700 °C (**Figs. 7 b, c**). At T_{tr} > 700 °C, the morphology of particles changes substantially (**Fig. 7 d**). They take a near-spherical shape and form aggregates/agglomerates of different size with signs of the primary sintering stage of particles.

The EDS analysis enables us to reveal the following features of the reconstruction of the elemental composition of the powders (**Fig. 8**): with increase in T_{tr}, the contents of O, Ca, and S change, which can be attributed to the reconstruction of $(CaSO_4 \cdot 2H_2O)_{sec}$into $(CaSO_4 \cdot 0.5\ H_2O)_{sec}$ and then into $CaSO_4$ at T_{tr}~ 900–1000 °C. The characteristic feature of such hard-burned powders is the difference in the content of elements in coarse and fine $CaSO_4$ particles. In the last-mentioned particles, the oxygen content turns out to be larger, whereas the sulfur content turns out to be smaller (**Fig. 9**). It can be concluded that this is caused by the beginning of the decomposition process of calcium sulfate, which is intensified with increase in temperature and will subsequently lead to the development of the reaction $2CaSO_4 \rightarrow 2CaO + 2SO_2\uparrow$, i.e., to the formation of the composite mixture $CaSO_4$+CaO (estrich gypsum). In **Fig. 7,** powders with a near-monophase composition are marked by arrows with the corresponding notation of phases. The changes in the contents of elements agree with the phase transformations established from the XRD data (see **Fig. 4**) and IR spectroscopy data (see **Fig. 5**).

The performed investigations show that the milled waste plaster molds are a polydisperse system consisting of a collection of particles and aggregates, whose size ranges from ~0.3 up to 300 μm. Phase transformations proceeding during temperature treatment of this powder somewhat differ from those for primary gypsum. A comparison of the temperature regions of phase transitions of primary and secondary $CaSO_4 \cdot 2H_2O$ (see **Figs. 5 a, c**) shows that the transformations into $CaSO_4 \cdot 0.5H_2O$ and $CaSO_4$ for gypsum waste is realized at higher temperatures than for primary gypsum. This fact can be explained by the following causes: the specific polydisperse composition of the used powder which usually formed at grinding of gypsum and cemented rockfill[23, 24], complicated egress of vapor and gases from dense aggregates of secondary calcium sulfate dehydrate [25] and by the presence of electrolytes penetrated into plaster molds from slips [26-28].

Phase transformations in large particles/agglomerates first occur in the surface layer of particles. Only with increase in T_{tr}, this process will be completed in the whole volume of particles. In particles with d< 1 μm, dehydration occurs faster. This is why, at T_{tr} > 200 °C, powders are usually a collection of particles of different phase composition. Nevertheless, powders formed at T_{tr} ~ 200–300 °C can be considered as soft-burned, whereas powders formed at T_{tr} = 1000 °C can be considered as hard-burned[29, 30]. The difference of these powders from the primary gypsum binders (see **Fig. 6 a**) calls for an investigation of their binding properties.

3.3. Binding properties of heat-treated powders of milled waste

Dough was prepared from powders subjected to temperature treatment. For the formation of dough of required consistency, different quantities of water are required (**Figs. 10 a–c**). As is seen in **Figs. 10 a, a'**, powders obtained at T_{tr}< 300 °C require the largest quantity of water. Correspondingly, the solidification of such blanks turns to be longer. The powders obtained at T_{tr}~ 1000 °C require the smallest quantity of water, and

setting of such blanks occurs faster. The obtained results agree with well-known data for soft- and hard-burned binders [31].

By introduction of a filler in the form of milled bottle cullet with $d \leq 70$ μm into gypsum powders, the water content required for the preparation of dough and the setting time of specimens are significantly decreased (**Figs. 10 b, b'**), which indicates the participation of surface defective layers of glass particles in the formation of new bonds responsible for the binding properties of newly formed gypsum [32-34].

Due to the preparation of mixtures with different contents of high-temperature and low-temperature powders and glass, it is possible to prepare dough with different water contents that sets for different time (**Figs. 10c, c'**). Note that, for the pottery and ceramic industry, the setting period of the gypsum (from the beginning to the end) is 6–30 min, whereas for other industries, the setting period of specimens can substantially change. As it follows from the data of **Figs. 10 a'–c'**, for our specimens, the setting time substantially increases. This can be caused by the penetration of electrolytes (liquid glass and sodium hydroxide) into plaster molds from clay slip. According to the EDS analysis data, the Na content in the plaster molds ranged from 0.08 to 0.14%, and the Si content in them ranged from ~0.17 to 0.45%.

3.4. Strength properties of specimens obtained from secondary soft– and hard-burned gypsum binders.

Since gypsum is extensively used in the building industry, in what follows the test results of several types of products, namely, blocks, plasterboards, and plastering, are presented.For the preparation of specimens from composite binders containing the soft-burned waste and hard-burned waste, preference was given to mixtures with a high content of soft-burned gypsum binder with T_{tr}= 300 ° C. As a hard-burned additive, gypsum waste after T_{tr}=1000 ° C were chosen, i.e.$CaSO_4$. Such a choice of the hard-burned mode was dictated by considerations of energy saving when obtaining a binder. Undoubtedly, the strength properties of products obtained with the use of estrich gypsum should be significantly higher. However, at the same time, energy consumption (gas or electricity) should increase significantly, since T_{tr}= 1200-1250 ° C is required.

In strength tests of blocks obtained from powders of heat-treated $(CaSO_4 \cdot 2H_2O)_{sec}$ powders (**Figs. 11 a, a'**), specimens subjected to high-temperature treatment (T_{tr}~ 1000 °C) exhibit the highest compressive strength and fracture toughness.

After the introduction of glass particles into the soft-burned binder (T_{tr} =300 °C) (**Figs. 11 b, b'**), the compressive strength and fracture toughness at $C_{glass} \leq$ 20 wt% turn out to be larger than those for specimens without glass additives. Similarresults were demonstrated in [35]. At a glass content above 20 wt%, the strength properties of specimens deteriorate. An analogous tendency is observed for specimens obtained from mixtures of soft-burned (T_{tr} =300 °C) and hard-burned (T_{tr} =1000 °C) gypsum binders $(CaSO_4 \cdot 2H_2O)_{sec}$ (**Figs. 11 c, c'**). The compressive strength and fracture toughness of these specimens depend substantially of the content of the hard-burned binder and decreases with increase in the content of the soft-burned gypsum binder in the composite powders.

The obtained values of the compressive strength of specimens made from the soft-burned binder containing $C_{glass} \leq$ 20 wt% and specimens made from hard-burned binder containing at most 20 wt% correspond to the strength of specimens made from primary gypsum plaster after setting for 2 h (4–6 MPa) and exceed 10 MPa after setting for a longer time. Such mixtures can be used for the manufacture of gypsum slabs whose compressive strength is 3.5–5 MPa and stucco molding and small art products.

From mixtures of secondary binders with additives of glass particles (i.e., in preparation of a composite gypsum binder) it is possible to obtain products of different strength. For example, gypsum plasterboard with satisfactory strength properties can be fabricated from the 60 wt% soft-burned gypsum binder + 20 wt% hard-burned gypsum binder + 20 wt% glass powder mixture (**Fig. 12**). Moreover, due to the additional introduction of disordered fibers of different organic origin and polymeric network, it is possible to substantially increase the strength properties of gypsum plasterboard [36, 37].

A strong coating, which in subsequent drilling has a relatively small fracture area can be obtained from (90–70) wt% soft-burned gypsum binder + hard-burned gypsum binder + (10–30) wt% glass powder mixtures (**Fig.**

13). A comparison of the sizes of the fracture areas of the coatings shows that glass particles with $d \sim 88$ μm favor the strengthening of the coating.

As noted in [38-40], the introduction of glass powder into concrete enhances substantially its strength. In our case, a similar effect is observed (see **Fig.10**). It is not improbable that, on the basis of highly defective surface layers of glass and anhydrite ($CaSO_4$) particles, compounds that impart additional binding properties to this material form. As a result, the deposited coating turns to be more resistant to the action of a water flow (rain).

IV. Conclusions

The performed investigations have shown that, during temperature treatment of $(CaSO_4 \cdot 2H_2O)_{sec}$ waste plaster molds from the ceramic industry, dehydration processes analogous to those proceeding in treatment of $(CaSO_4 \cdot 2H_2O)_{primary}$ occur. However, the temperature of the phase transitions $(CaSO_4 \cdot 2H_2O)_{sec} \rightarrow (CaSO_4 \cdot 0.5H_2O)_{sec}$, and $(CaSO_4 \cdot 0.5H_2O)_{sec} \rightarrow CaSO_4$ is shifted to the region of higher temperatures by ~100-150 °C, whereas high-temperature treatment at 900–1000 °C is characterized by only the beginning of the destruction of the crystal lattice of $CaSO_4$. For the formation of CaO, a treatment temperature $T_{tr} > 1100$ °C is required. Soft- and hard-burned powders and their mixtures (composite powders) exhibit good binding properties.

By choosing the contents of the soft- and hard-burned gypsum binders in the composites and introducing additives of milled glass, it is possible to change the water consumption in preparation of tough, the setting time of products, and their strength properties.

On the basis of newly-formed soft-burned (200–300 °C) and hard-burned (1000 °C) gypsum binders (composite mixtures), it is possible to obtain small products (stucco molding, art products), blocks, plasterboard, and plaster possessing good strength properties without using primary gypsum binders.

The obtained results indicate the possibility of complete processing of waste plaster molds from the ceramic industry, which are an important element of environmental contamination because of the large volume output of sanitary and household ceramics.

References

[1] Karni, J., Karni, E. (1995) Gypsum in construction: origin and properties. *Mater. Struct.*28**,** 92–100. https://doi.org/10.1007/BF02473176.

[2] Gypsum: Properties, Poduction and Application, 2011. Ed. Sampson, D.H. Nova Science Publishers Inc., New York, 371 pp.

[3] The Gypsum Construction Handbook, 2014. 7th Edition, Willey, USG, ISBN: 978-1-118-74984-5 2014. 576 p.

[4] Sophia, M., Sakthieswaran, N., Ganesh Babu, O. (2016) Gypsum as a construction material-review of recent developments.*Int. j. innov. res. sci. eng. technol*. (IJIRST) 2 (12), 315-323.

[5] Lushnikova, N., Dvorkin, L. (2016) Sustainability of gypsum products as a construction material, In book: Sustainability of Construction Materails, 2nd edition 2016, Chapter 25, pp.643-682. Ed. Khatib Jamal. Publisher: Woodhead Publishing. DOI: 10.1016/B-978-0-08-100370-1.00025-1

[6] Cressey G., Minerals-Sulfates (2005) Encyclopedia of Geology, Elsevier, pp. 572-573.

[7] Vrancken, K.C., Laethem, B. (2000) Recycling options for gypsum from construction and demolition waste. *Waste Manage. Series*, 1, 325-331.https://doi.org/10.1016/S0713-2743(00)80045-8

[8] Garg, M., Jain, N. (2010) Waste gypsum from intermediate dye industries for production of building materials.*Constr. Build. Mater.*24[9], 1632-1637. DOI:10.1016/j.conbuildmat.2010.02.029.

[9] Viana, E.T., Ribeiro, L., Lintz, R.C.C., Gachet-Barbosa, L.A., Pires, M.S.G., 2013. Management of **g**ypsum in **c**onstruction **s**ite - **c**ase **s**tudy,*Appl. Mech. Mater.*405-408, 3119-3122.DOI:10.4028/www.scientific.net/AMM.405-408.3119

[10] Geraldo, R.H.S., Pinheiro, M.M., Silva, J.S., Andrade, H.M.C., Dweck, J., Gonçalves, J.P., Camarini, G. (2017) Gypsum plaster waste recycling: A potential environmental and industrial solution. *J. CleanerProd.* 164, 288-300. https://doi.org/10.1016/j.jclepro.2017.06.188

[11] Wiss, J., Camp, T., Ladoo, R. (1930) Gypsum plaster in the ceramic industries.*J. Am. Ceram. Soc*., 13, 287-314.doi: 10.1111/j.1151-2916.1930.tb16271.x

[12] Nikolaev, D.P. (2013) Molding gypsums in the production of ceramic sanitary and table ware. Adapted porosity with optimal strength. *Glass Ceram.* 70, 311–312. https://doi.org/10.1007/s10717-013-9569-7

[13] Pishch, I.V., Klimosh, Y.A., Gapanovich, E.I. (2006) Flow properties of slip for producing ceramic sanitary ware. *Glass Ceram.* 63**,** 259–261. https://doi.org/10.1007/s10717-006-0093-x

[14] ASTM C 472 – 99.Standard test methods for physical testing of gypsum, gypsum plasters and gypsum concrete. ASTM C472-99, Standard Test Methods for Physical Testing of Gypsum, Gypsum Plasters and Gypsum Concrete, ASTM International, West Conshohocken, PA, 1999. DOI: 10.1520/C0472-99R09

[15] ASTMC1421-0.9.Standard test methods for determination of fracture toughness of advanced ceramics at ambient temperature.DOI:10.1520/C1421-10.

[16] Kilic, A.M., Kilic, Ö. (2007) The phase transition in natural gypsum, *Asian J. Chem.*, 19 [4], 3157-3168.

[17] Kuntze, R.A. (2009) Gypsum: connecting science and technology, ASTM MNL 67, ASTM International. ISBN 978-0-8031-7015-5

[18] Bensted, J., Varma, S.P. (1971) Infrared spectroscopic studies of calcium sulphate heated to high temperatures. *Z. Naturforsch. B*, 26, 690-693.

[19] Yang Liu, Alian Wang, Freeman J.J. (2009) Raman, Mir, and Nir spectroscopic study of calcium sulfates: gypsum, bassanite, and anhydrite. 40th Lunar and Planetary Science Conference. https://www.lpi.usra.edu/meetings/lpsc2009/pdf/2128.pdf

[20] Bishpo, J.L., Lane, M.D., DarbyDyar, M., King, S.J., Brown, A.J., Swayzem, G. (2014) Spectral properties of Ca-sylfates:gypsum, bassanite and anhydrite, *Am. Mineral*. 5-14. DOI: http//dx.doi.rg/10.2138/am-2014-4756.

[21] NhiThao Ngoc Le, Ngoc ThuyTrang Le, Quang Lam Nguyen, Truc Le-Buu Pham, Minh-Tri Nguyen-Le, Dai Hai Nguyen (2020) A facile synthesis process and evaluations of α-calcium sulfate hemihydrate for bone substitute, *Materials (Basel)*. 13(14), 3099, 1-13. doi: 10.3390/ma13143099.

[22] Zaki, M.I., Knozinger, H., Tesche, B., Mekhemer, G.A.H. (2006) Influence of phosphonation and phosphation on surface acid-base and morphological properties of CaO as investigated by in situ FTIR spectroscopy and Electron Microscopy. J. Colloid and Interface Science, 303[1], 9-17. https://doi.org/10.1016/j.jcis.2006.07.011

[23] Wu J.Y., Feng M.M., Mao X.B., Xu J.M., Zhang W.L., Ni X.Y., Han G.S. (2018) Particle size distribution of aggregate effects on mechanical and structural properties of cemented rockfill: Experiments and modeling. *Constr. Build. Mater*. 193, 295–311. doi: 10.1016/j.conbuildmat.2018.10.208.

[24] Koper, A., Prałat, K., Ciemnicka, J., Buczkowska, K. (2020) Influence of the calcination temperature of synthetic gypsum on the particle size distribution and setting time of modified building materials.*Energies*, 13, 5759. https://doi.org/10.3390/en13215759

[25] López, F.A.; Tayibi, H.; García-Díaz, I.; Alguacil, F.J. (2015) Thermal dehydration kinetics of phosphogypsum. Mater de Construcc. 65 [319] e061.http://dx.doi.org/10.3989/mc.2015.07214.

[26] Leskeviciene, V., Sarlauskaite, I., Nizeviciene, D., Kybartiene, N. (2010) Influence of theGypsumDehydration temperature and alkali additives on the properties of anhydrite cement, Sci. Sintering, 42, 233-243. doi: 10.2298/SOS1002233L UDK 621.742:621.89.099:622.785.

[27] Sari M., Leksellent J. (2002) Regulation of the setting and hardening of mineral binders. Mix. Build. SPb.: 2-5 December.

[28] Petropavlovskaya, V.B. (2018) Non-fired gypsum composites with improved performance properties, Thesis D. Sci., Tver, Russia (in Russian).

[29] Freyer, D., Voigt, W. (2003) Crystallization and phase stability of $CaSO_4$ and $CaSO_4$-based salts, *Monatsh. Chem.* 134[5], 693-719. DOI: 10.1007/s00706-003-0590-3.

[30] Vimmrová, A., Krejsová, J., Scheinherrová, L., Doleželová, M., Keppert, M. (2020) Changes in structure and composition of gypsum paste at elevated temperatures. *J. Therm. Anal. Calorim.*142,19–28. https://doi.org/10.1007/s10973-020-09528-8.

[31] Ferronskay, A., 2004.Gypsum materials and products (Production and use).IzdatelstvoAssotsiatsiiStroitel'nyhVuzov, Moscow, 488 pp. (in Russian). Cod: 223178. ISBN: 5-93093-272-7.

[32] RakeshSakale, Sourabh Jain, Seema Singh, 2016. Experimental Investigation on Strength of Glass Powder Replacement by Cement in Concrete with Different Dosages.International Journal of Science Technology and Engineering (IJSTE), 2 (08), 76-86.

[33] Gómez-Soberón, J.M., Cabrera-Covarrubias, F.G., Almaral-Sánchez, J.L., Consolación Gómez-Soberón, M. (2018) Fresh-state properties of mortars with recycled glass aggregates: global unification of behavior. *Adv. Mater. Sci. Eng.* Article ID 1386946,11 p. https://doi.org/10.1155/2018/1386946

[34] Veena V., Bhat , N., BhavanishankarRao. Influence of Glass Powder on the Properties Of Concrete, International Journal of Engineering Trends and Technology (IJETT), V16(5),196-199 Oct 2014. ISSN:2231-5381. www.ijettjournal.org. published by seventh sense research group.

[35] Shepel, S.V., GhaziWakili, K., Hugi E. (2012) Investigation of heat transfer in gypsum plasterboard exposed to fire for three nominal fire scenarios, *J. Fire Sci.* 30 (3), 240–255. DOI: 10.1177/0734904111433265

[36] Serna A., del Rio M., Palomo J. G., Gonzalez, M. (2012) Improvement of gypsum plaster strain capacity by the addition of rubber particles from recycled tyres. *Contr. Buil. Mater.*35, 633-641. https://doi.org/10.1016/j.conbuildmat.2012.04.093

[37] Rajabipour, F., Maraghechi, H., Fischer, G. (2010) Investigating the alkali silica reaction of recycled glass aggregates in concrete materials. *J. Materi Civ. Eng.*, 22 [12], 1201-1208. DOI: 10.1061/ (ASCE)MT.1943-5533.0000126.

[38] Bhat, V.V., BhavanishankarRao N. (2014) Influence of glass powder on the properties of concrete. International Journal of Engineering Trends and Technology (IJETT), 16 [5], 196-199.DOI: 10.14445/22315381/IJETT-V16P242

[39] Patel, A., Trivedi, A., Shah, R. (2016) Effects on compressive strength of concrete by using glass powder as replacement of cement. *Int. J. Eng. Res. Technol.* (IJERT), 5 [04]. ID: IJERTV5IS040974.

[40] Renuka G.M., Melinamani, S., Nadaf, A., Pawar, A., Allipur, B.S. (2020) Partial replacement of fine aggregate by glass powder. International Journal of Futures Research and Development (IJFRD), 1 [1], 89-98. https://ubipayroll.com/IJFRD/index.php/ijfrd/article/view/53

Figure captions

Figure 1: Working scheme of obtaining $CaSO_4 \cdot 0.5H_2O$ and use of molds for slip casting in the ceramic industry.

Figure 2:. Processing scheme of gypsum waste.

Figure 3: Change in the size of $(CaSO_4 \cdot 2H_2O)_{sec}$ particles with increase in the milling rate at a milling time t = 3 min (a) and with increase in the milling time at v = 300 rpm (b). In (c): particle-size distribution after milling in the regime: v = 300 rpm, t = 5 min. In (c'): particle-size distribution after ultrasonic destruction.

Figure 4:XRD patterns of $(CaSO_4 \cdot 2H_2O)_{sec}$ powder heat treated in the temperature range 100–1000 °C.
Figure 5: FTIR spectra of $(CaSO_4 \cdot 2H_2O)_{sec}$ powders subjected to temperature treatment: (a) in the range 4000–500 cm^{-1}; (b) in the range 1150–500 cm^{-1}.
Figure 6: Comparative schemes of phase transformations of $CaSO_4 \cdot 2H_2O$.
Figure 7: SEM micrographs of the initial waste powders (a) and after treatment at different temperatures T_{tr} (b–c).
Figure 8: Distribution of elements in waste particles after treatment at different temperatures T_{tr} on a square of sizes 9.556 × 9.556 μm^2according to EDS data.
Figure 9: Distribution of elements in waste particles after treatment at T_{tr}= 1000 °C according to EDS data.
Figure 10:. Water absorption (a–c) and time of complete setting of gypsum dough (a'–c') vs. the treatment temperature of the $(CaSO_4 \cdot 2H_2O)_{sec}$ powder (a, a'), vs. the content of glass additives to the $(CaSO_4 \cdot 2H_2O)_{sec}$ powder treated at 300 °C (b, b'); vs. the content of $(CaSO_4 \cdot 2H_2O)_{secondary}$ powder treated at 300 °C in mixtures with the $(CaSO_4 \cdot 2H_2O)_{sec}$ powder treated at 1000 °C (c–c').

Figure 11: The ultimate compressive strength (a–c) and fracture toughness (a'–c') vs. the treatment temperature of $(CaSO_4 \cdot 2H_2O)_{sec}$ powder (a, a'), vs. the content of glass additives to the $(CaSO_4 \cdot 2H_2O)_{sec}$ powder treated at 300 °C (b, b'), vs. the content of the $(CaSO_4 \cdot 2H_2O)_{sec}$ powder treated at 300 °C in mixtures with the $(CaSO_4 \cdot 2H_2O)_{sec}$ powder treated at 1000 °C (c–c'). The results were obtained after setting for 4 days.

Figure 12: Change in the compressive strength (a) and fracture toughness (b) of specimens after setting for 7 days.

Figure 13: Change in the size of the fracture area of a coating containing glass particles of different sizes (a). In (b) and (c): change in the size of the fracture area of the coating vs. the diameter of a drill. In (a): d_{drill} = 0.47 cm. In (b): the gypsum coating does not contain glass particles. In (c): d_{glass} = 88 μm.

Figure 14: Scheme of the influence of rain on the gypsum coating (a) and the amount of material removed from the coating containing different amounts of glass particles with d_{glass} = 88 μm (b).

T_{tr}, °C	**ν, cm^{-1}**						Absorption bands assignment
Gypsum waste	3527.2sh **3401.5w,wd**	2978.4vw	1683.3w 1619.4w	**1103.7st,n** 1004.2sh	667m,n	596.3m,n	Bands at ν ~ 3500 cm^{-1}, 1600 cm^{-1} belong O-H bonds; band in region ν ~ 1084- 1095 cm^{-1} belongs to antisisymetricstrech vibration modes of SO_4tetrahedra; bands in region ν ~ 674-590 cm^{-1} belong to antisymmetric bending vibrations of SO_4tetrahedra.
100	3612sh **3546.4w,wd** 3405sh	2978.2vw	1619.4w,n	1141.5sh 1109.6sh **1084.9st,n** 1007.5sh	**659.2m,n**	627.1sh **596.2m,n**	
200	3612w	2977.6vw	1618.5w,n	1168.3sh 1141.2sh 1112.1sh **1086.1st,n** 1007.6sh	**659.1m,n**	627.2sh **596.3m,n** 551.4sh 538.2sh	
300	3610.6vw	2979.6vw	1620.2w	1142.2sh 1111.4sh **1089.5st,n** 1009.3sh	**671.4m,n** 659.5sh	611.5sh **592.6m,n**	
400				1140.9sh **1094.6st,n** 1106.1sh 1010.7sh	**672m,n** 660.1sh	610.6sh **593m,n**	
500				1145.2sh **1093.6st,n** 1014sh	**671.1m,n**	610.2sh **591.9m,n**	
600				1219.1sh 1146.9sh **1095.1st,n** 1014.3sh	**671.9m,n**	610.5sh **592.6m,n**	
700				1220.2sh 1146.5sh 1106.1sh **1094.5st,n** 1014.2sh	**672.3m,n**	611sh **592.3m,n**	
800				1217.1sh 1130.3sh **1094.3st,n** 1014.1sh	**674.2m,n**	610.1sh **592.3m,n**	
900				1216sh 1126.8sh **1094.3st,n** 1014sh	**674.2m,n**	610.2sh **592.4m,n**	
1000				1221.3sh 1150sh 1126.3sh **1094.5st,n** 1013.8sh	**672.4m,n**	609.1sh **591.2m,n**	

Table 1. Position of IR absorption bands in gypsum wastes subjected to temperature treatment.

Note: **st.** means strong; **m** means middle; **w** means weak; **n** means narrow; **wd** means wide; **sh** means shoulder; **v** means very

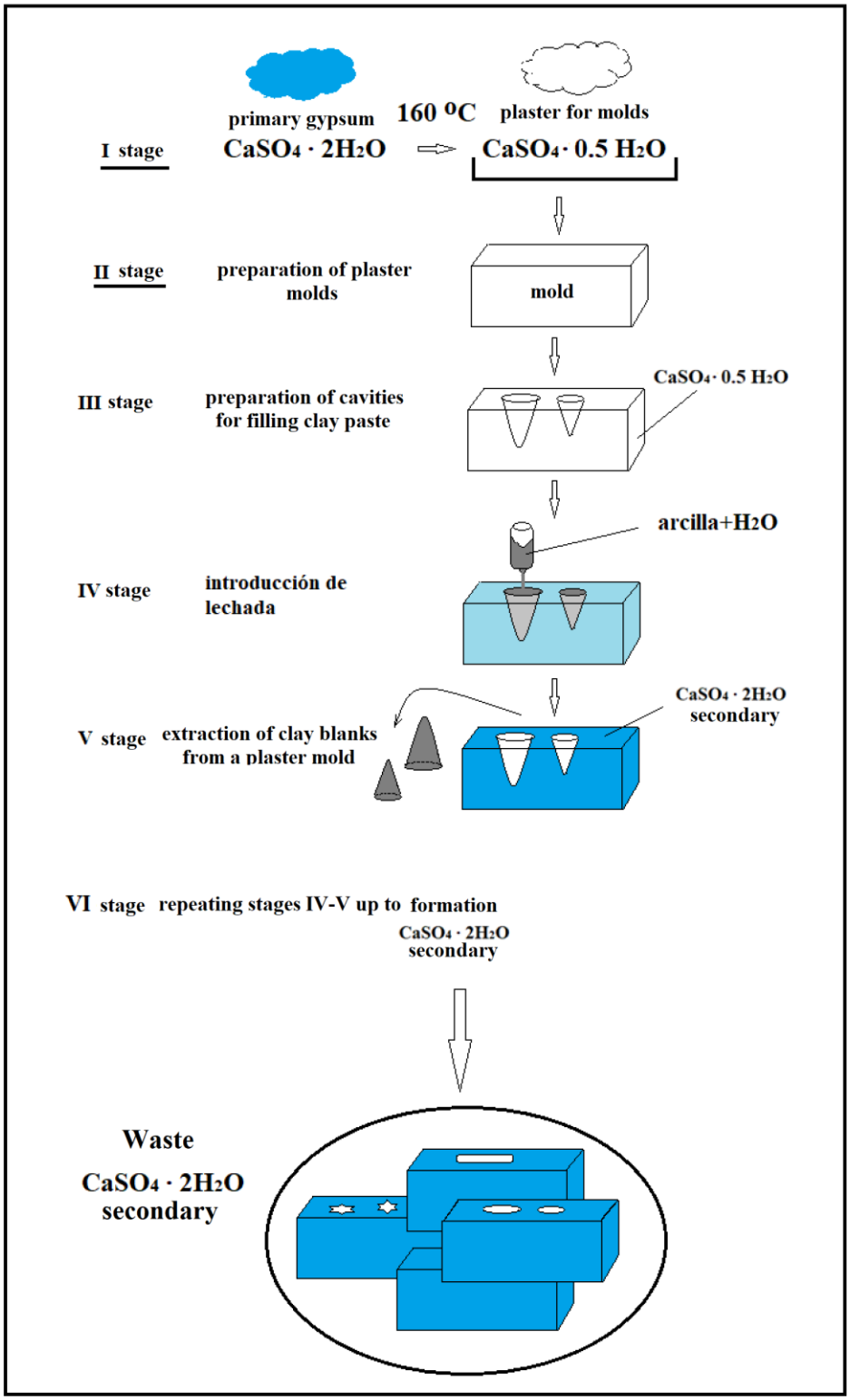

Fig. 1. Working scheme of obtaining $CaSO_4 \cdot 0.5H_2O$ and use of molds for slip casting in the ceramic industry.

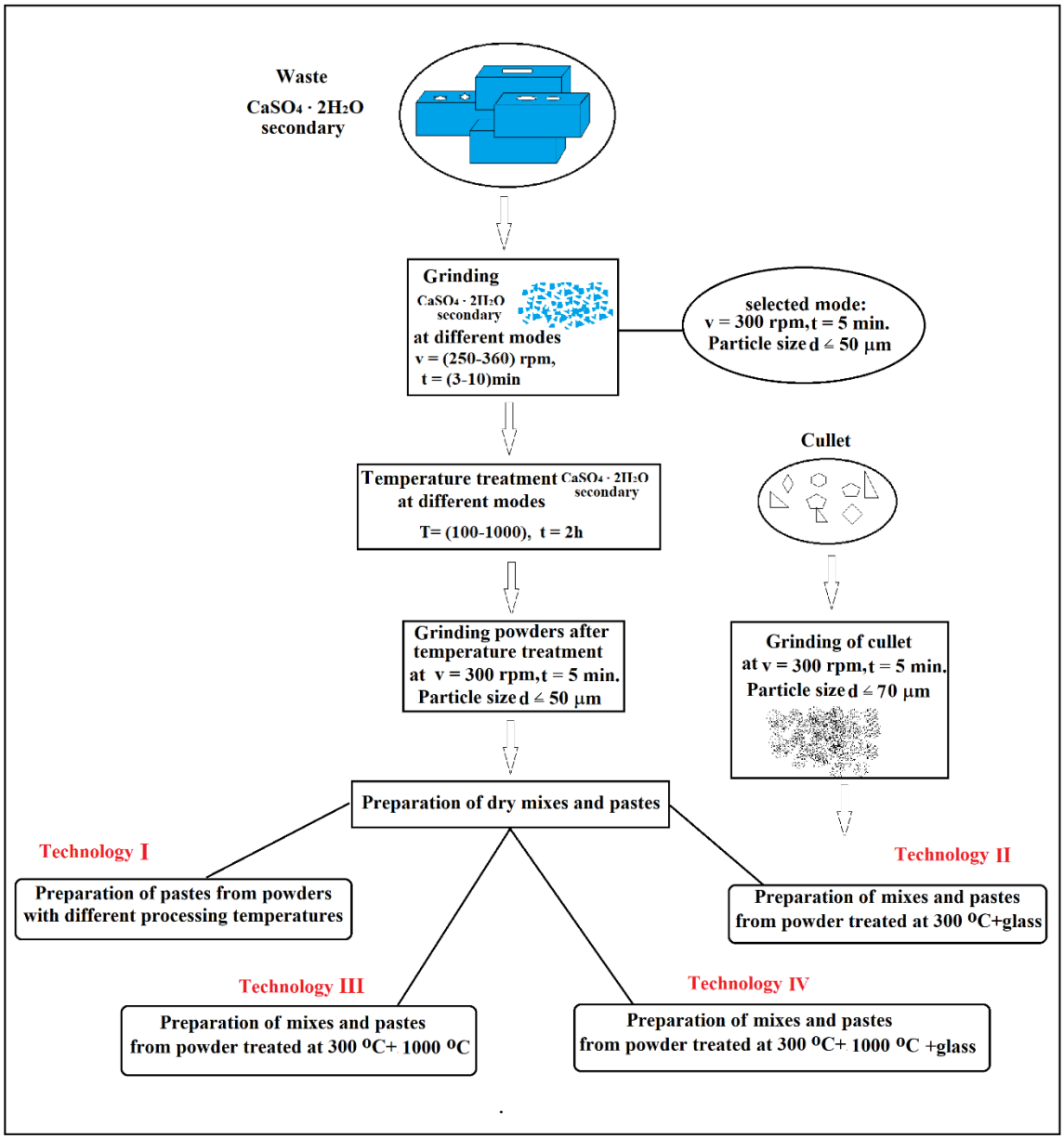

Fig. 2. Processing scheme of gypsum waste.

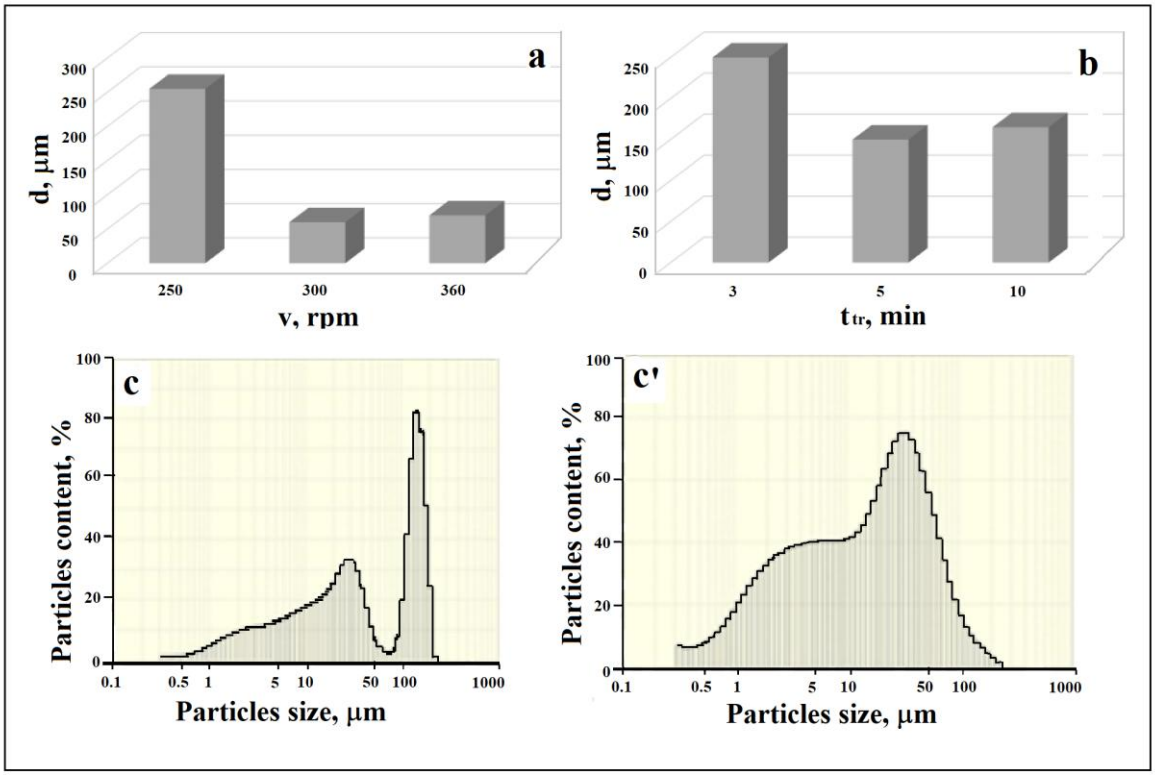

Fig. 3. Change in the size of $(CaSO_4 \cdot 2H_2O)_{sec}$ particles with increase in the milling rate at a milling time t = 3 min (a) and with increase in the milling time at v = 300 rpm (b). In (c): particle-size distribution after milling in the regime: v = 300 rpm, t = 5 min. In (c'): particle-size distribution after ultrasonic destruction.

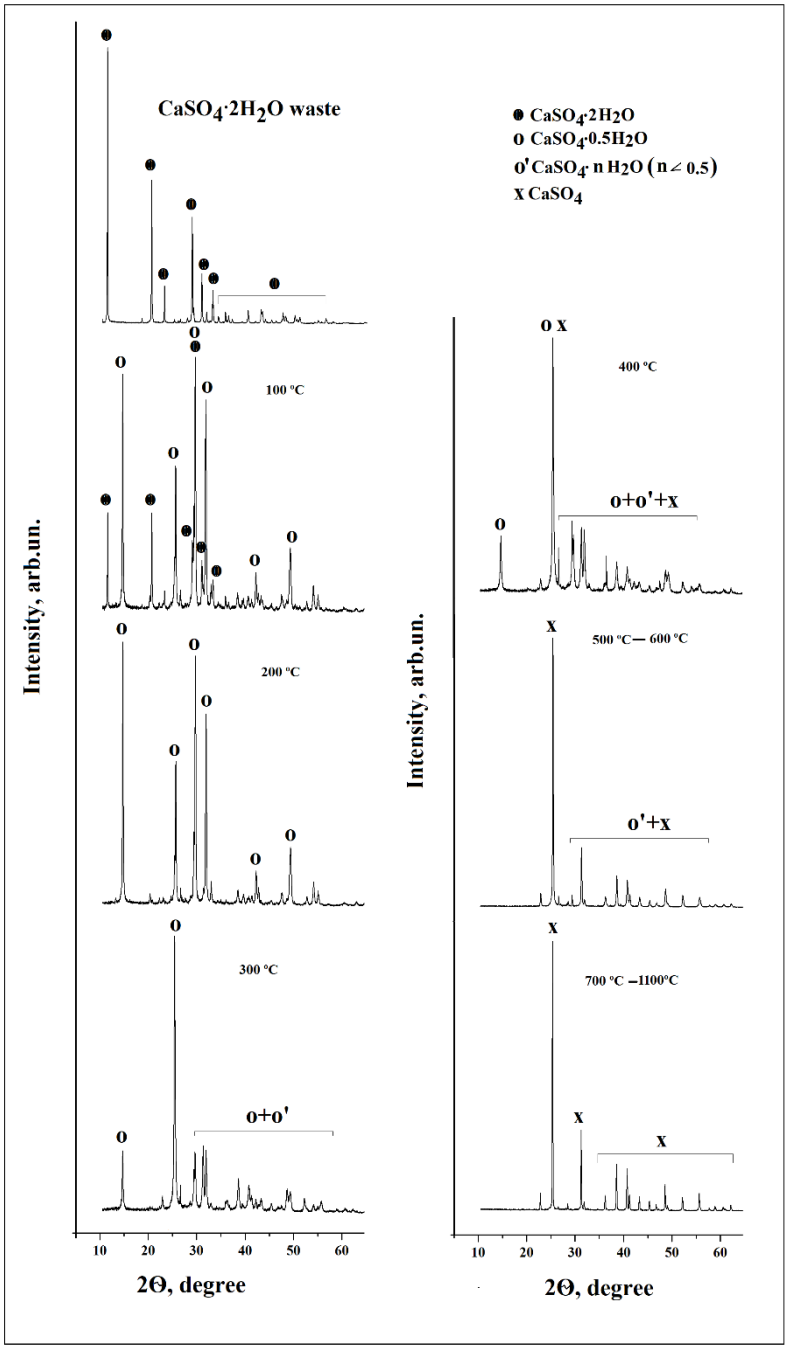

Fig. 4. XRD patterns of $(CaSO_4 \cdot 2H_2O)_{sec}$ powder heat treated in the temperature range 100–1000 °C.

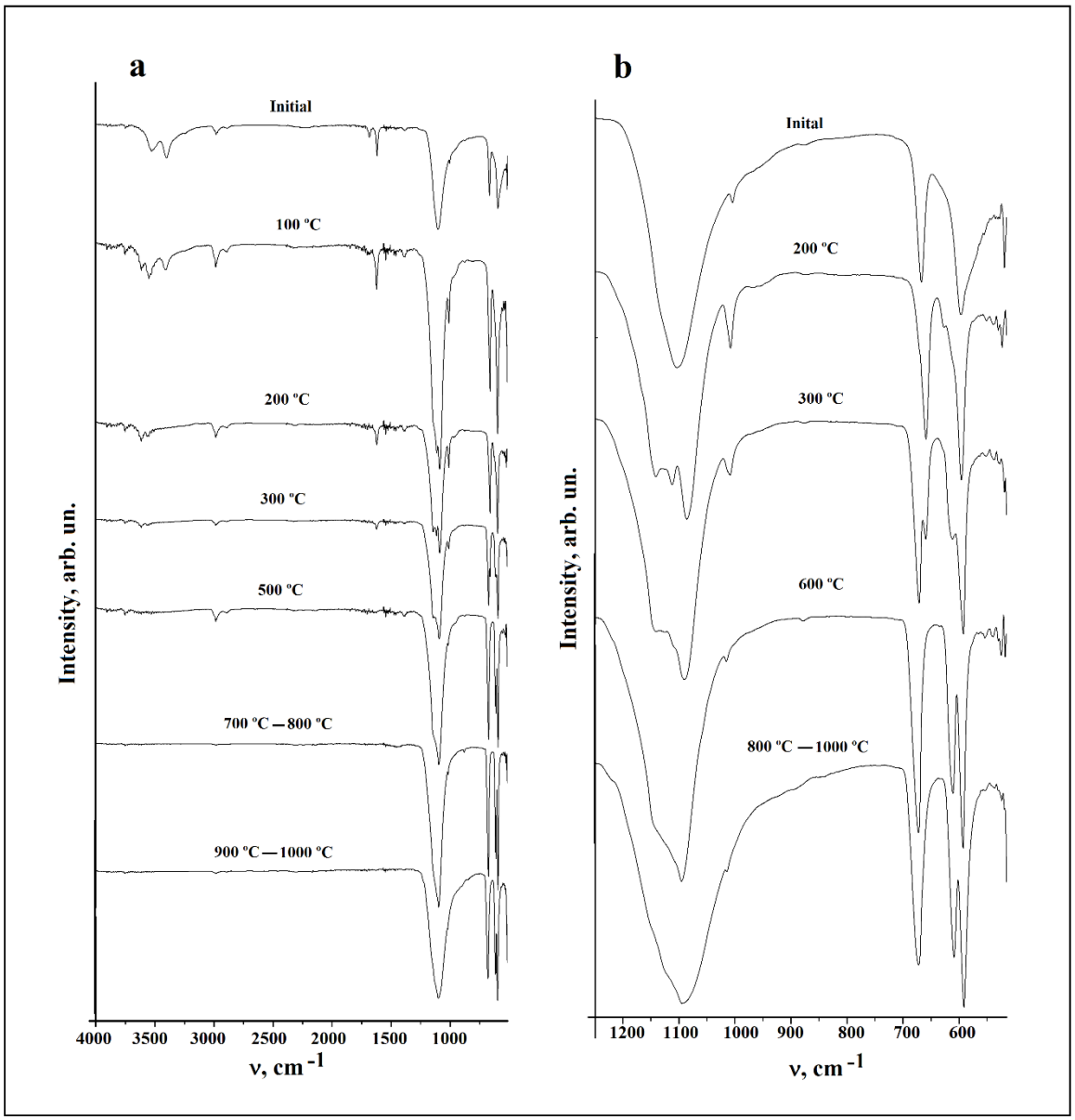

Fig. 5. FTIR spectra of $(CaSO_4 \cdot 2H_2O)_{sec}$ powders subjected to temperature treatment: (a) in the range 4000–500 cm^{-1}; (b) in the range 1150–500 cm^{-1}.

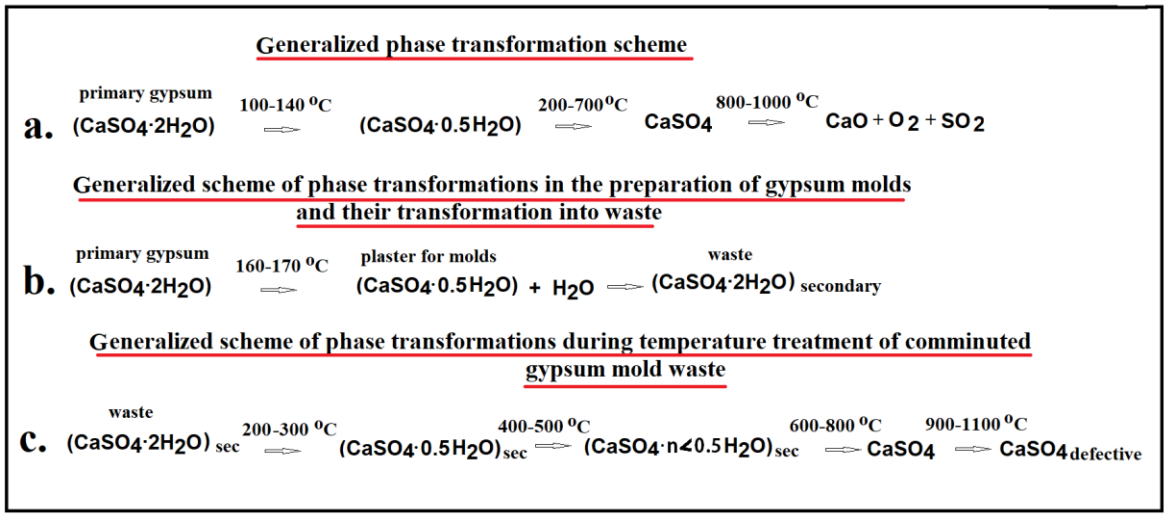

Fig. 6. Comparative schemes of phase transformations of $CaSO_4 \cdot 2H_2O$.

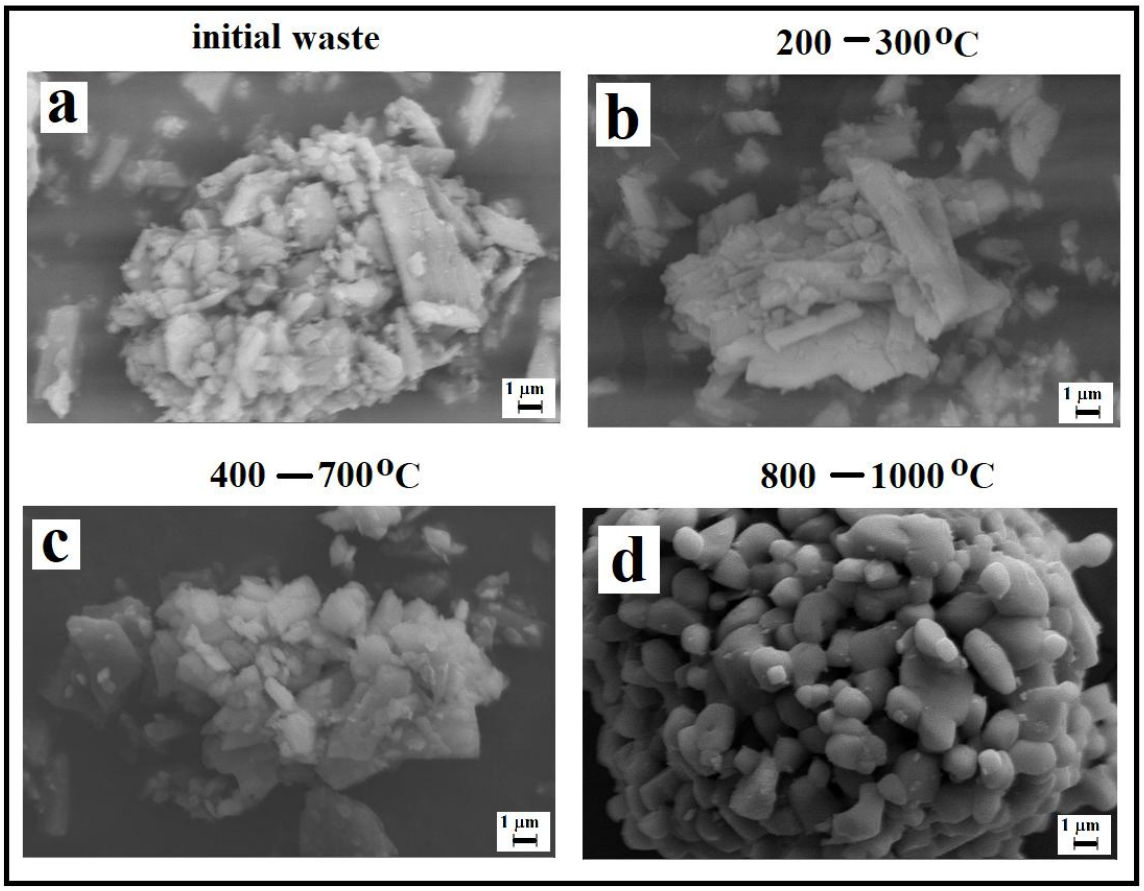

Fig. 7. SEM micrographs of the initial waste powders (a) and after treatment at different temperatures T_{tr} (b–c).

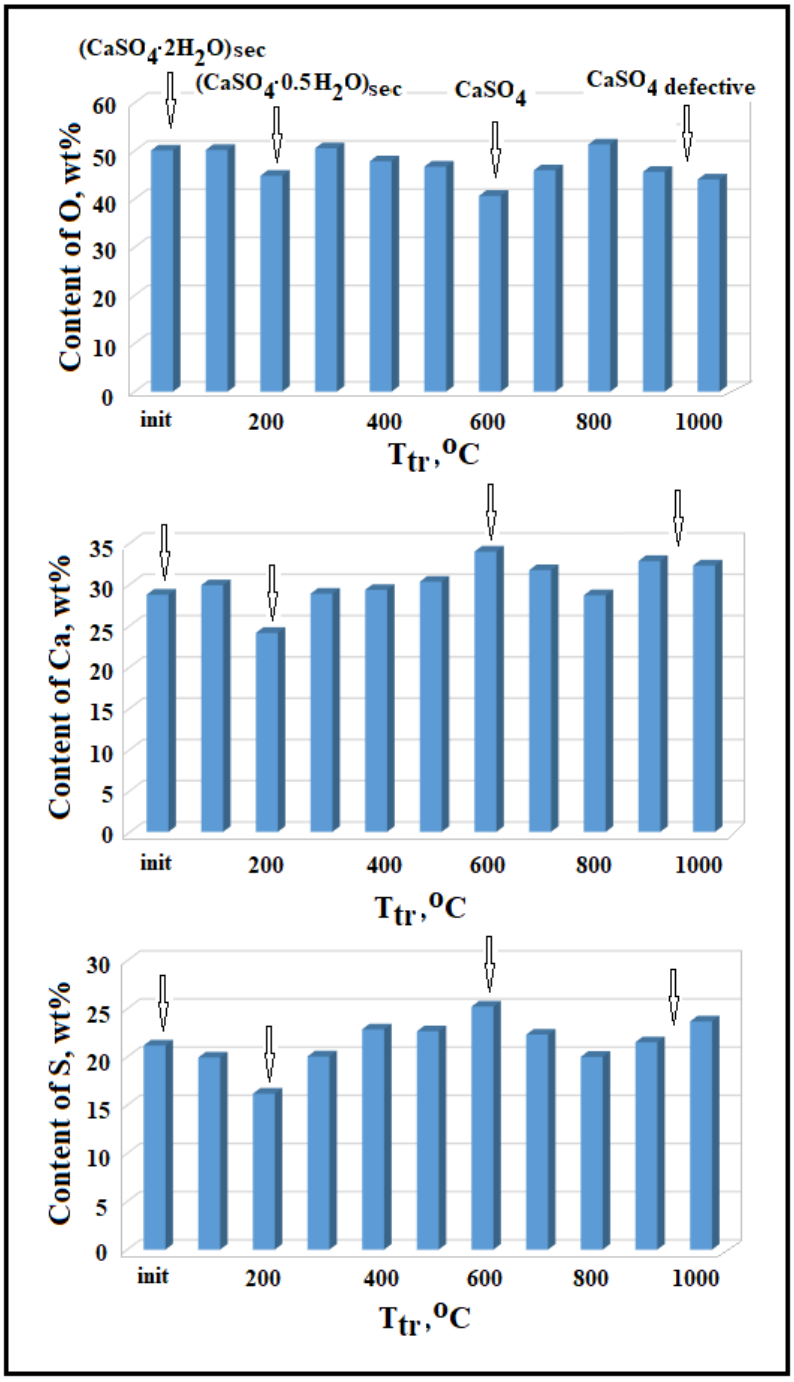

Fig. 8. Distribution of elements in waste particles after treatment at different temperatures T_{tr} on a square of sizes 9.556 × 9.556 μm^{2}according to EDS data.

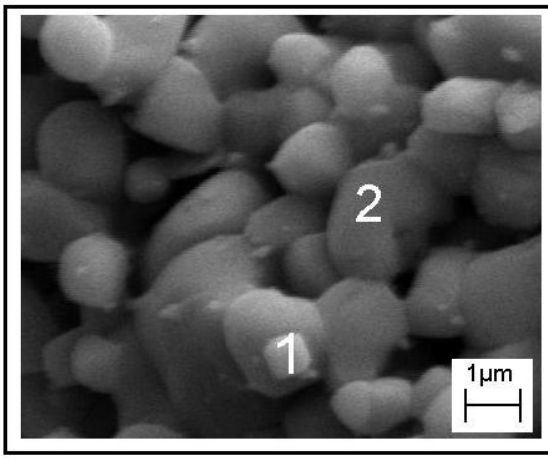

	Element	Weight%
1	O	56.69
	S	18.84
	Ca	24.47
2	O	52.09
	S	20.59
	Ca	27.32

Fig. 9. Distribution of elements in waste particles after treatment at T_{tr}= 1000 °C according to EDS data.

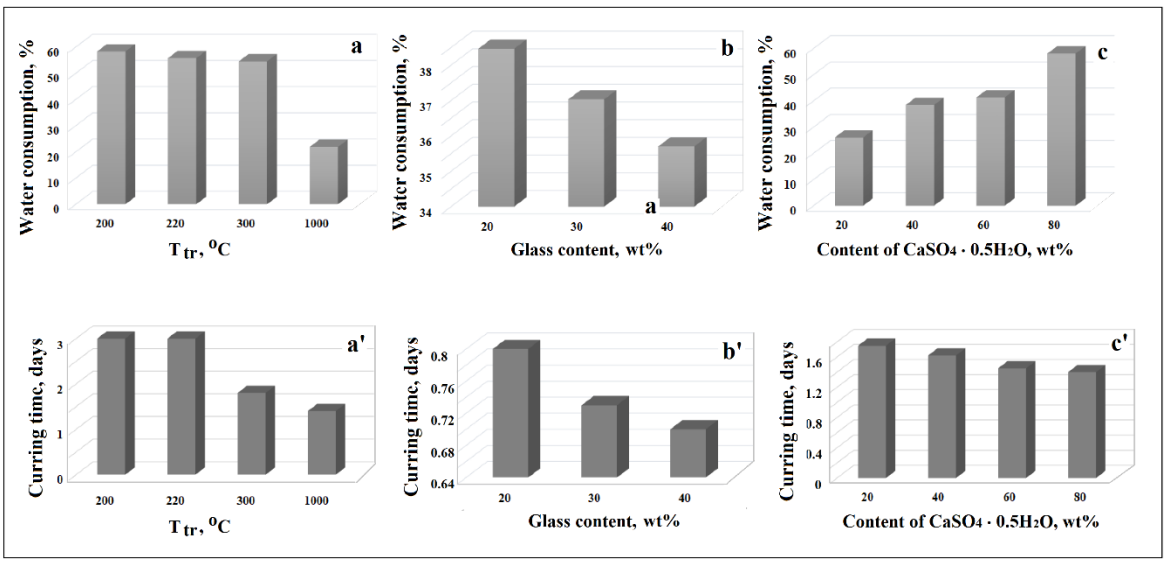

Fig. 10. Water absorption (a–c) and time of complete setting of gypsum dough (a'–c') vs. the treatment temperature of the $(CaSO_4 \cdot 2H_2O)_{sec}$ powder (a, a'), vs. the content of glass additives to the $(CaSO_4 \cdot 2H_2O)_{sec}$ powder treated at 300 °C (b, b'); vs. the content of $(CaSO_4 \cdot 2H_2O)_{sec}$ powder treated at 300 °C in mixtures with the $(CaSO_4 \cdot 2H_2O)_{sec}$ powder treated at 1000 °C (c–c').

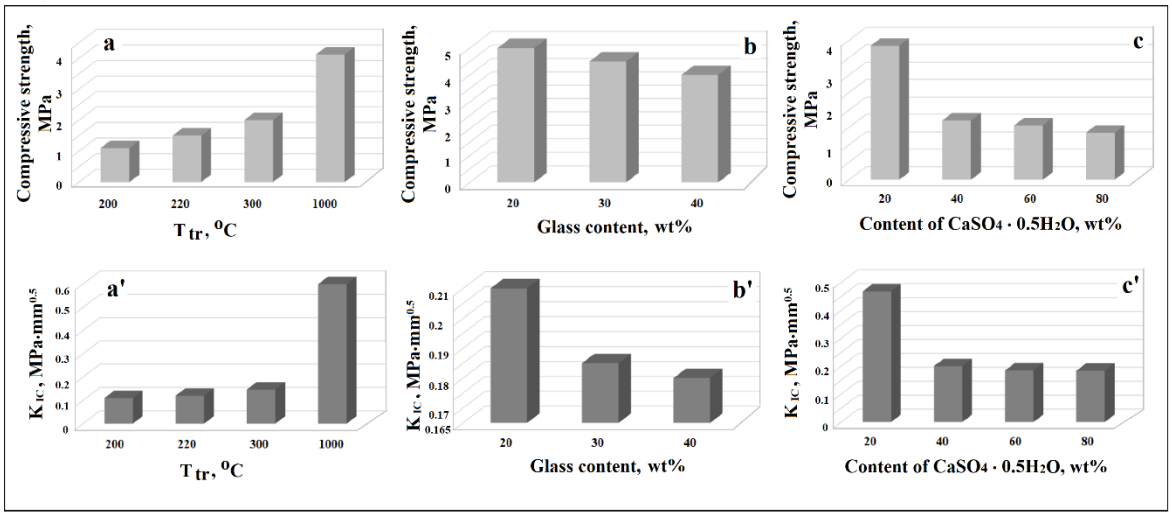

Fig. 11. The ultimate compressive strength (a–c) and fracture toughness (a'–c') vs. the treatment temperature of $(CaSO_4 \cdot 2H_2O)_{sec}$ powder (a, a'), vs. the content of glass additives to the $(CaSO_4 \cdot 2H_2O)_{sec}$ powder treated at 300 °C (b, b'), vs. the content of the $(CaSO_4 \cdot 2H_2O)_{sec}$ powder treated at 300 °C in mixtures with the $(CaSO_4 \cdot 2H_2O)_{sec}$ powder treated at 1000 °C (c–c'). The results were obtained after setting for 4 days.

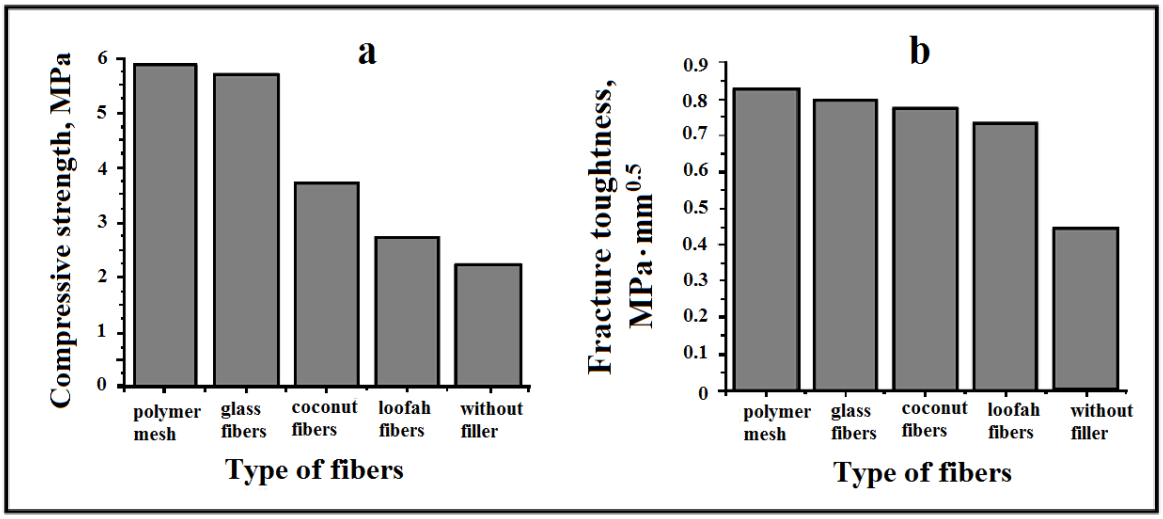

Fig. 12. Change in the compressive strength (a) and fracture toughness (b) of specimens after setting for 7 days.

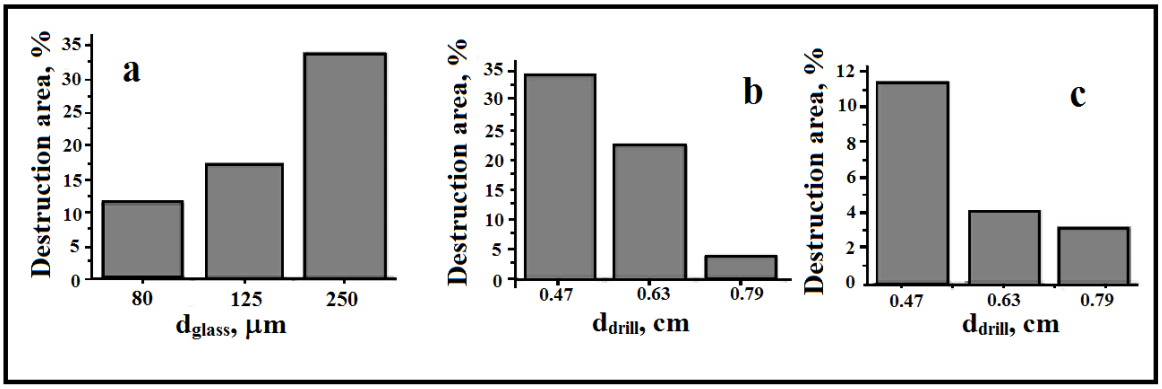

Fig. 13. Change in the size of the fracture area of a coating containing glass particles of different sizes (a). In (b) and (c): change in the size of the fracture area of the coating vs. the diameter of a drill. In (a): d_{drill} = 0.47 cm. In (b): the gypsum coating does not contain glass particles. In (c): d_{glass} = 88 μm.

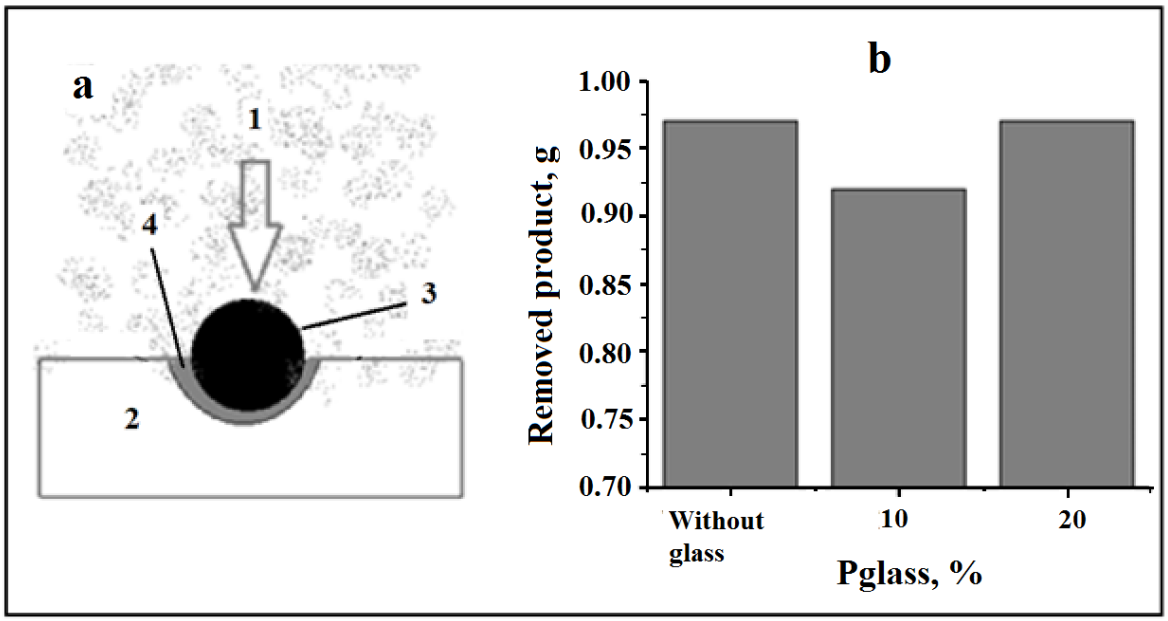

Fig. 14. Scheme of the influence of rain on the gypsum coating (a) and the amount of material removed from the coating containing different amounts of glass particles with d_{glass} = 88 μm (b).